# Thermally induced optical bistability in Cr-doped Colquiriite crystals

M. A. Noginov,* M. Vondrova, and B. D. Lucas
*Center for Materials Research, Norfolk State University, 700 Park Ave., Norfolk, VA 23504*
(Received 28 November 2000; published 27 December 2001)

We have shown that a very strong nonlinearity in the temperature dependence of the luminescence quantum yield in Cr-doped laser crystals of the Colquiriite family can lead to a temperature induced intrinsic optical bistability in these materials. The bistability and the hysteresis loop in the dependence of Cr luminescence intensity and transmission of the crystal on cw pumping power has been theoretically predicted and experimentally observed. The experimental results are in a good qualitative and quantitative agreement with the theoretical prediction.

DOI: 10.1103/PhysRevB.65.035112 PACS number(s): 78.20.−e, 42.65.Pc, 42.70.−a, 42.70.Hj

## I. INTRODUCTION

A phenomenon of optical bistability, when certain parameters of a nonlinear system have two stable states, was first reported by Gibbs *et al.* in 1976.[1] Phenomena of optical bistability in the systems without cavity form a special group of *intrinsic* bistability effects, first discussed in dense media by Bowden and Sung.[2] Potential applications of optical bistability include all-optical logic elements and switches for optical computing, telecommunication, etc.

An intrinsic optical bistability can be theoretically predicted in various systems when a complexity of a nonlinear equation describing the system is high enough. The physical mechanisms of nonlinearity that induce bistability may be very different. For example, the bistability in Refs. 3 and 4 was derived as a consequence of modification of the optical Bloch equations after introducing the local field correction terms. This type of bistability, enhanced by cooperative upconversion, has been experimentally observed in several $Yb^{3+}$ doped dielectric crystals.[5–9] Intrinsic bistability can potentially be observed in laser-related crystals and glasses with complex energy transfer schemes, energy upconversion, avalanche excitation, etc.

In this work, we theoretically predict and experimentally demonstrate the effect of intrinsic optical bistability in luminescence and transmission of a system (Cr-doped $LiSrGaF_6$ or $LiSrAlF_6$ Colquiriite crystals) where one of its parameters, luminescence quantum yield, has a strongly nonlinear dependence on temperature.

*Cr-doped Colquiriite crystals.* Cr:LiSGaF ($Cr^{3+}$:$LiSrGaF_6$) and Cr:LiSAF ($Cr^{3+}$:$LiSrAlF_6$) are known as efficient active media for broad-band tunable and femtosecond mode-locked lasers.[10–13] These crystals are members of the Colquiriite family along with LiCaF ($LiCaAlF_6$), LiSCaF ($LiCa_xSr_{1-x}AlF_6$), and LiChrom ($LiSrCrF_6$). Cr-doped crystals with the Colquiriite structure have been reported to have a very strong dependence of the lifetime and the luminescence quantum yield on temperature.[14] In these materials, the rate of radiationless relaxation strongly increases with temperature after certain critical point determined by the host material.

Cr:LiSGaF has two broad absorption bands centered near 440 and 640 nm. They arise from the $^4A_2 \rightarrow {}^4T_1 a$ and the $^4A_2 \rightarrow {}^4T_2$ transitions of $Cr^{3+}$. The emission spectra are due to the $^4T_2 \rightarrow {}^4A_2$ transition. The emission peak occurs near 0.83 $\mu$m. Because Cr:LiSGaF is an uniaxial crystal, the absorption and emission spectra differ when the incident light is polarized parallel or perpendicular to the crystallographic axis *c* of the crystal.[10]

In the crystals of the Cr:LiSGaF family, in addition to the radiative decay (spontaneous emission), there are two other radiationless decay mechanisms: energy transfer upconversion and phonon induced nonradiative decay. The process of energy transfer upconversion in Cr:LiSGaF and Cr:LiSAF involves the interaction of two excited Cr ions in their $^4T_2$ states.[15] In this process one ion is promoted to the higher energy level $^4T_1$ while the other is transferred to its $^4A_2$ ground state. The $^4T_1$ excitation is followed by the radiationless relaxation back to the $^4T_2$ state. Upconversion is essentially important at high pumping densities, when the concentration of the excited Cr ions is high, and in heavily doped crystals where the average distance between Cr ions is small.

According to Stadler *et al.*,[14] the phonon induced nonradiative decay in Cr-doped Colquiriite crystals is primarily possible because the level crossing of the $^4T_2$ excited state with the $^4A_2$ ground state lies relatively close to the minimum of the $^4T_2$ excited state (point A, Fig. 1). In this arrangement, the occupied $^4T_2$ vibrational excited states above the crossing point can be very efficiently depopulated by tunneling to very high lying vibrational levels of the electronic ground state $^4A_2$.[14] At low temperatures, the nonradiative decay rate is negligibly small in comparison with the radiative decay. However, when at high temperatures the rate of nonradiative decay becomes higher than the rate of the radiative decay, one observes a strong luminescence quenching and decrease in the emission lifetime.

In Cr-doped LiSGaF and LiSAF crystals the increase in temperature due to a laser pumping causes the increase of radiationless relaxation rate and the reduction of the luminescence quantum yield. This, in turn, initiates a stronger heat extraction, which causes the further growth of the temperature, that leads again to the increase of the heat extraction rate, etc. In general, the same sequence of processes can be found in almost all laser-related solid-state materials. However, in Cr:LiSGaF and Cr:LiSAF crystals, very strong temperature dependence of the luminescence lifetime makes the effect especially prominent. The contributions from different relaxation channels to the heat extraction in Cr-doped Col-

 

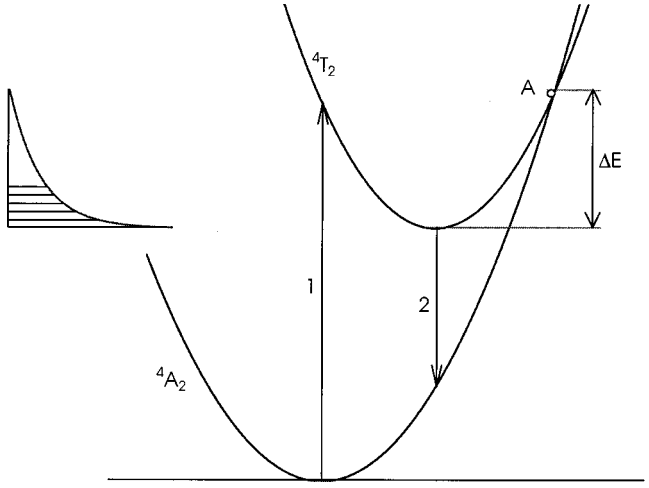


FIG. 1. Schematic diagram of the energy levels in Cr-doped Colquiriite crystals. 1: absorption, 2: emission, $\Delta E$: the energy gap between the crossing level of the $^4T_2$ and $^4A_2$ states (point A) and the minimum of the $^4T_2$ excited state. Inset: Boltzmann population of the $^4T_2$ vibrational states.

quiriites were studied in detail in Ref. 16.

## II. LIFETIME MEASUREMENTS IN Cr:LiSGaF AND Cr:LiSAF

Experimentally, we have recorded the emission decay kinetics in Cr(1.5%):LiSGaF and Cr(1.5%):LiSAF (The Cr:LiSGaF and Cr:LiSAF crystals used in this work were kindly provided by Arlete Cassanho, who is currently with AC Materials, Inc.) at the temperatures varying between the 295 and 575 K. The crystals were excited with 532 nm $Q$-switched laser pulses ($t_{\text{pulse}} \approx 10$ ns). The power density of the laser excitation was kept low, so the influence of upconversion in our experiment was negligibly small. The emission signal was detected at $\lambda \approx 830$ nm. The emission kinetics were nearly single exponential. The plots of experimentally determined decay times vs temperature are shown in Fig. 2. The experimental curves could be perfectly fitted with the formula

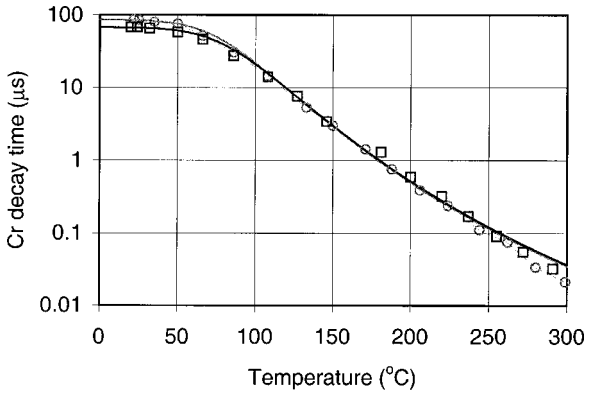


FIG. 2. Luminescence decay time plotted vs temperature in Cr(1.5%):LiSGaF (circles) and Cr(1.5%):LiSAF (squares). Solid lines: best fit curves calculated according to formula (1).

$$\tau^{-1} = A + B \exp(-\Delta E/kT), \tag{1}$$

where $A$ is the radiative decay rate assumed to be temperature independent, $\Delta E$ is the energy gap between the minimum of the $^4T_2$ excited state and the crossing point of the $^4T_2$ excited state with the $^4A_2$ ground state (Fig. 1), $T$ is the temperature, $k$ is Boltzmann constant, and $B$ is a preexponential factor.

From the experimental dependence of the emission lifetime on temperature, we have determined in Cr:LiSGaF, $A = 1.16 \times 10^4\ \text{s}^{-1}$, $B = 8 \times 10^{12}\ \text{s}^{-1}$, and $\Delta E/kT_{\text{room}} = 24.3$. The corresponding parameters in Cr:LiSAF were found to be $A = 1.47 \times 10^4\ \text{s}^{-1}$, $B = 7.5 \times 10^{12}\ \text{s}^{-1}$, and $\Delta E/kT_{\text{room}} = 24.25$. Here, $T_{\text{room}}$ is the room temperature equal to 296 K.

## III. THEORETICAL MODELING

The theoretical modeling of optical bistability in Cr:LiSGaF and Cr:LiSAF was based on the following assumptions.

(1) The excited volume in the sample is pumped uniformly, both in the direction of the light propagation and in the cross section of the laser beam.

(2) The heat sink has the constant temperature $T_0$, unchanged during the experiment.

(3) The rate of the heat transfer to the chiller, $dQ/dt$, is proportional to $\Delta T = T - T_0$, where $T$ is the temperature of the pumped volume. The coefficient of proportionality between $dQ/dt$ and $\Delta T$, dependent on the thermal conductivity coefficient and the geometry of the experiment (size of the sample, size of the pumped area, distance from the pumped area to the heat sink, etc.) is $\chi$ (in W/deg).

(4) The heat sinking conditions are the same for the entire pumped volume.

(5) The change of pumping power in the experiment is very slow. That is why we neglect in the heat balance the term proportional to the specific heat capacity of the material. In this approximation, the heat balance is determined entirely by the heat deposition and the heat sinking.

(6) The luminescence decay mechanisms include (a) the radiative decay rate $nA$, where $n$ is the concentration of excited Cr ions, (b) the rate of upconversion given by of $\alpha n^2$, where $\alpha$ is the upconversion constant, and (c) phonon-induced nonradiative decay described as $nB \exp(-\Delta E/kT)$.

(7) The quantum yield of absorbed excitation from the level $^4T_1$ to the luminescent level $^4T_2$ is assumed to be equal to unity.

(8) The temperature dependence of the radiative decay constant $A$ and the upconversion constant $\alpha$ is neglected in comparison with the temperature dependence of the exponential term $B \exp(-\Delta E/kT)$.

Under these assumptions, the following three steady state equations describing the heat balance and the excited state concentration in the system can be used to create a model predicting the bistable behavior of Cr:LiSGaF and Cr:LiSAF:

$$0=\frac{dQ}{dt}=W_a\left(1-\eta\frac{\nu_e}{\nu_p}\right)-(T-T_0)\chi, \tag{2a}$$

$$\eta=\frac{A}{A+\alpha n+B\exp(-\Delta E/kT)}, \tag{2b}$$

$$0=\frac{dn}{dt}=\frac{W_a}{h\nu_p ls}-nA-\alpha n^2-nB\exp(-\Delta E/kT), \tag{2c}$$

where $Q$ is the heat energy, $W_a$ is the absorbed pumping power, $\eta$ is the quantum yield of luminescence, $\nu_e$ is the average frequency of the spontaneous emission, $\nu_p$ is the frequency of the pumping light, $h$ is Planck constant, $l$ is the length of the crystal in the direction of the pumping beam, and $s$ is the cross section area of the pumped volume.

Equation (2a) describes the heat balance in the system. In this equation, $(1-\eta\nu_e/\nu_p)$ is the portion of absorbed pumping energy that does not leave the system in form of luminescence but is deposited in the crystal in form of heat, and $(T-T_0)\chi$ is the rate of the heat sinking. The luminescence quantum yield is defined by Eq. (2b) and the balance of the excited state concentration is described by Eq. (2c), where $W_a/h\nu_p ls$ represents the increase in the excited state concentration due to the absorbed pumping $W_a$.

The system of stationary Eqs. (2a), (2b), (2c) has one physically allowed solution for $n$ as a function of $W_a$ and $T$:

$$n=\frac{\sqrt{\left(y^2+\frac{4\alpha W_a}{h\nu_p ls}\right)}-y}{2\alpha}, \tag{3}$$

where $y=A+B\exp(-\Delta E/kT)$ and one physically allowed solution for $W_a$ as a function of $T$:

$$W_a=\frac{-b+\sqrt{(b^2-4ac)}}{2a}, \tag{4}$$

where

$$a=\frac{\alpha}{A^2h\nu_p ls},$$

$$b=\frac{2(T_0-T)\chi\alpha}{A^2h\nu_p ls}-\left(\frac{\nu_e}{\nu_p}\right)^2+\frac{1}{A}\left(\frac{\nu_e}{\nu_p}\right)y,$$

and

$$c=\frac{(T_0-T)^2\chi^2\alpha}{A^2h\nu_p ls}+\frac{(T_0-T)\chi}{A}\left(\frac{\nu_e}{\nu_p}\right)y.$$

In our modeling, we first calculated the absorbed pumping $W_a$ as a function of the temperature $T$, and the excited state concentration $n$ as a function of $W_a$ and $T$. Then, we plotted $n$ against $W_a$ using the temperature $T$ as a parameter.

Several parameters in the system can be changed experimentally. The heat sink temperature $T_0$ can be varied by changing the temperature of the cold finger in the cryostat. The ratio $\nu_e/\nu_p=\lambda_p/\lambda_e$ can be varied by changing the pumping wavelength $\lambda_p$. (In Cr:LiSGaF, the central weighed emission frequency corresponds to 11 990 $cm^{-1}$.) The heat sinking factor $\chi$ can be modified by changing the distance between the pumped volume and the heat sink, the size of the pumped spot, the geometry of the sample, the efficiency of the heat sink contacts, etc. The cross section area of the pumped volume $s$ can be changed by focusing the beam. The upconversion coefficient $\alpha$ can be varied by choosing crystals with different Cr concentrations.

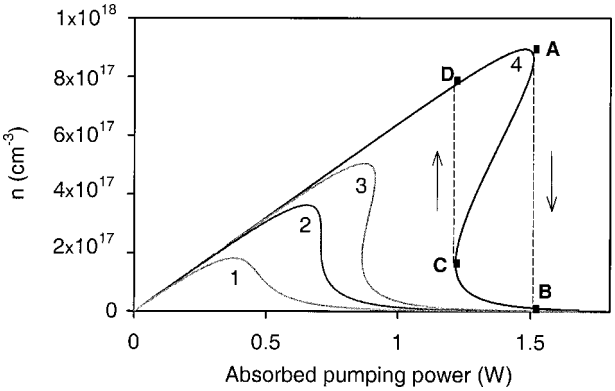


FIG. 3. Calculated excited state concentration $n$ vs absorbed power $W_a$ at different temperatures $T_0$. 1: $T_0=300$ K, 2: $T_0=270$ K, 3: $T_0=250$ K, 4: $T_0=200$ K; $\alpha=1\times10^{-18}$ $cm^3/s$, $\lambda_p=488$ nm, $\chi=6\times10^{-3}$ W/deg, $l=0.1$ cm, $s=3.3\times10^{-3}$ $cm^2$.

The calculations were done at the parameters $A$, $B$, $\Delta E$, and $\alpha$ corresponding to those in Cr:LiSGaF. Since these parameters and the temperature behavior of the luminescence lifetime are close to those in Cr:LiSAF, the model predictions discussed below are valid for Cr:LiSAF as well.

In Fig. 3, the calculated excited state concentration $n$ is plotted versus the absorbed pumping power $W_a$ for several different heat sink temperatures. One can see from this figure that at room temperature only one value of steady-state concentration corresponds to each pumping power (trace 1). However, at lower temperatures the $n(W_a)$ curves have a region where three values of $n$ correspond to each pumping power (traces 2, 3, and 4). The multiple-state solutions correspond to an ''inverse *S*-shape'' part of the curve. The solutions between points $A$ and $C$ are inherently unstable. Two other steady solutions, between points $D$ and $A$ and between points $B$ and $C$, are stable and physically allowed.

When the pumping power is very slowly increased, starting from weak pumping powers, the excited state concentration (and luminescence intensity) will increase following the upper branch of the curve until it reaches point $A$, where the slope $dn/dW_a$ is equal to $-\infty$. At this point the excited state concentration will abruptly switch to the solution corresponding to the lower branch of the curve (point $B$) and follow it as the pumping power is increased further. The switch is indicated in Fig. 3 by the vertical dashed line. When the pumping is slowly reduced from its maximum value (above point $B$), the excited state concentration will follow the lower branch until it reaches point $C$, where the slope $dn/dW_a$ is equal to $+\infty$. At this point, $n$ will switch to the solution on the upper branch (point $D$) and then follow the upper branch at the further decrease of the pumping power. Thus, the hysteretic behavior and intrinsic bistability

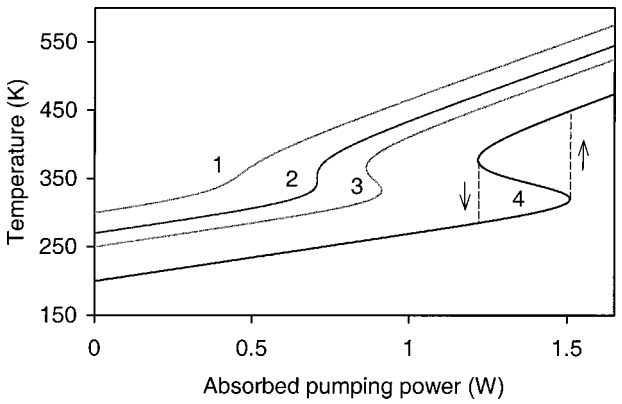


FIG. 4. Calculated internal temperature $T$ vs absorbed power at different heat sink temperatures $T_0$. 1: $T_0=300$ K, 2: $T_0=270$ K, 3: $T_0=250$ K, 4: $T_0=200$ K; $\alpha=1\times10^{-18}$ cm$^3$/s, $\lambda_p=488$ nm, $\chi=6\times10^{-3}$ W/deg, $l=0.1$ cm, $s=3.3\times10^{-3}$ cm$^2$.

are predicted in Cr steady state luminescence in Cr:LiSGaF and Cr:LiSAF crystals.

As follows from Fig. 3, the size of the hysteresis loop (in both $W_a$ and $n$ dimensions) as well as the critical power required for the switch to occur increases with the decrease of the heat sink temperature $T_0$.

The series of the corresponding temperature traces is plotted vs absorbed pumping power in Fig. 4. Similarly to the $n(W_a)$ curves, no bistability in the $T(W_a)$ plots is observed until the heat sink temperature is lowered down to approximately 270 K. At lower heat sink temperatures both bistability and hysteresis emerge in the power dependence of the temperature of the pumped spot. Again, the size of the hysteresis loop and the critical switching temperature increase with the decrease of $T_0$. The comparison of Fig. 3 and 4 shows that the hysteresis and the abrupt switch between two stable states occur simultaneously in the $n(W_a)$ and $T(W_a)$ curves.

Figure 5 shows the effect of the ratio $\lambda_e/\lambda_p$ on the shape of the curve. While there is almost no bistability predicted at $\lambda_p=488$ nm at $T_0=270$ K, the hysteretic effect is very

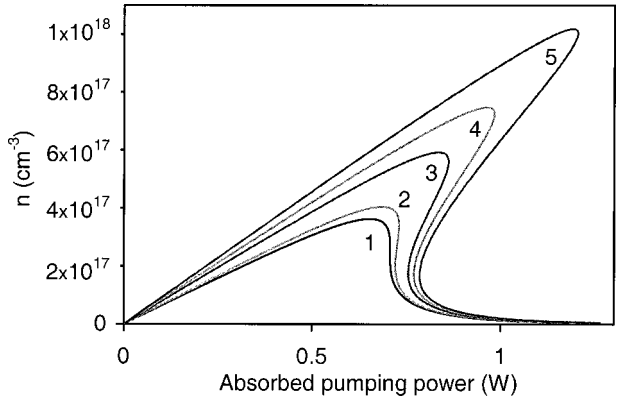


FIG. 5. Calculated excited state concentration $n$ vs absorbed power $W_a$ at different pumping wavelength. 1: $\lambda_p=488$ nm, 2: $\lambda_p=514$ nm, 3: $\lambda_p=600$ nm, 4: $\lambda_p=647$ nm, 5: $\lambda_p=700$ nm; $\alpha=1\times10^{-18}$ cm$^3$/s, $\chi=6\times10^{-3}$ W/deg, $T_0=270$ K, $l=0.1$ cm, $s=3.3\times10^{-3}$ cm$^2$.

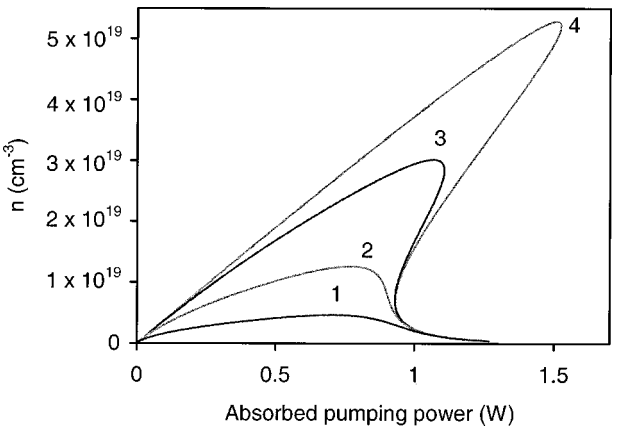


FIG. 6. Calculated excited state concentration $n$ vs absorbed power $W_a$ at different $\alpha$. 1: $\alpha=10^{-14}$ cm$^3$/s, 2: $\alpha=10^{-15}$ cm$^3$/s, 3: $\alpha=10^{-16}$ cm$^3$/s, 4: $\alpha=10^{-17}$ cm$^3$/s, $T_0=250$ K, $\lambda_p=700$ nm, $\chi=6\times10^{-3}$ W/deg, $l=0.1$ cm, $s=7.8\times10^{-5}$ cm$^2$.

strong at $\lambda_p=700$ nm. As follows from the figure, the closer the pumping wavelength to the emission wavelength, the stronger the bistability effect is. Thus, at the wavelength of a red diode laser ($\lambda_p\approx650$ nm), the hysteresis loop can be observed even at room temperature.

Figure 6 shows the plots of $n$ vs $W_a$ calculated for different values of the upconversion parameter $\alpha$. As follows from this figure, upconversion lowers the value of cw excited state concentration of Cr ions and suppresses the hysteresis and bistability. Consequently, the reduction of the diameter of the pumped spot, which increases the effect of upconversion in the crystals with reasonably high Cr concentration, suppresses the effect of hysteresis and bistability as well. (According to Ref. 17, in Cr:LiSGaF, $\alpha=1\times10^{-16}$ cm$^3$/s corresponds to the Cr concentration $n_{\mathrm{Cr}}=1.5\%$, $\alpha=2\times10^{-16}$ cm$^3$/s corresponds to $n_{\mathrm{Cr}}=3\%$, $\alpha=9\times10^{-16}$ cm$^3$/s corresponds to $n_{\mathrm{Cr}}=10\%$, $\alpha=10^{-15}$ cm$^3$/s corresponds to $n_{\mathrm{Cr}}=20\%$, and $\alpha=2\times10^{-15}$ cm$^3$/s corresponds to $n_{\mathrm{Cr}}=100\%$.)

The shape of the $n(W_a)$ curve remains unchanged with the variation of the heat sinking factor $\chi$. However, both $n$ and $W_a$ values scale proportionally to $\chi^{-1}$. So, the change of $\chi$ affects the effective size of the curve, Fig. 7.

As follows from Fig. 8, in Cr:LiSGaF crystal, the absorption coefficient in the blue-green spectral region $k_{\mathrm{abs}}$ increases with the increase of temperature. At $\lambda=488$ nm and the light polarization $E\|c$, we extrapolated the experimental dependence $k_{\mathrm{abs}}(T)$ with the formula $k_{\mathrm{abs}}=c\cdot n_{\mathrm{Cr}}\cdot(0.003T-0.272)$, where $n_{\mathrm{Cr}}$ was Cr concerntration in at.% and $c$ was the polarization factor ($c=1$ at $E\perp c$ and $c=2/3$ at $E\|c$).

Since the absorption coefficient and the absorbed pumping power $W_a$ depend on the temperature $T$ and $T$ has a hysteretic behavior as a function of $W_a$, the absorbed power $W_a$ and the transmitted power $W_t$ should demonstrate the hysteretic behavior and bistability when plotted versus incident pumping power $W_i$, Fig. 9. Thus, we predicted that the intrinsic optical bistability in Cr:LiSGaF could be observed not only in the luminescence but also in the transmitted light intensity.

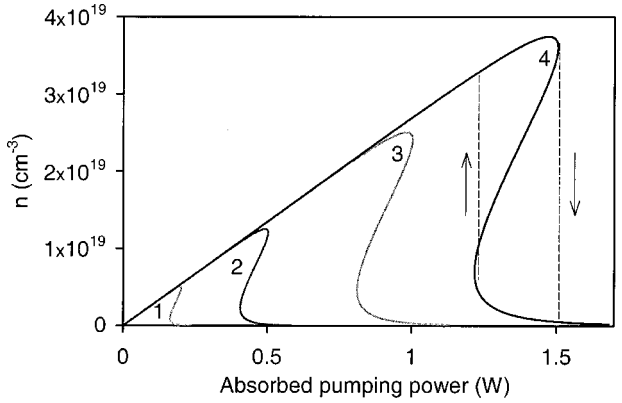


FIG. 7. Calculated excited state concentration $n$ vs absorbed power $W_a$ at different $\chi$. 1: $\chi=8\times10^{-4}$ W/deg, 2: $\chi=2\times10^{-3}$ W/deg, 3: $\chi=4\times10^{-3}$ W/deg, 4: $\chi=6\times10^{-3}$ W/deg; $\alpha=10^{-18}$ cm$^3$/s, $T_0=200$ K, $\lambda_p=488$ nm, $l=0.1$ cm, $s=7.8\times10^{-5}$ cm$^2$.

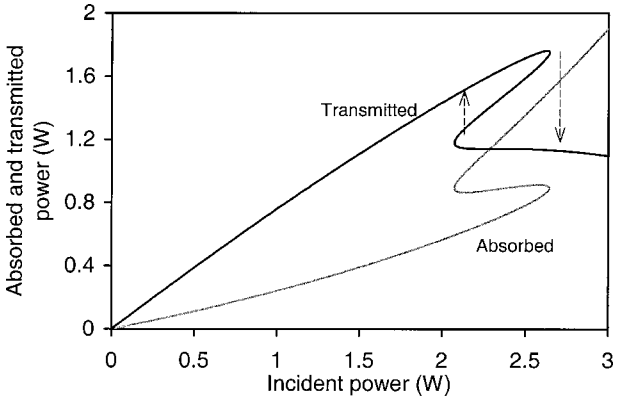


FIG. 9. Calculated absorbed and transmitted power vs incident power. $\alpha=10^{-18}$ cm$^3$/s, $\lambda_p=488$ nm, $\chi=6\times10^{-3}$ W/deg, $l=0.1$ cm, $s=3.3\times10^{-3}$ cm$^2$, $T_0=250$ K, $n_{\mathrm{Cr}}=8.5\%$, $E\parallel c$.

Consequently, the dependence of the cw excited state concentration $n$ on the incident power $W_i$ (Fig. 10) looks differently from the dependence of $n$ on the absorbed power $W_a$. The size of the hysteresis loop is larger when $n$ is plotted as a function of $W_i$ rather than a function of $W_a$. Curiously enough, the closed loop can be predicted in the dependence $n(W_i)$ at low temperatures (Fig. 10, trace 5). However, the part of the curve between points $A$ and $B$ (corresponding to the part of the curve between points $A$ and $C$ in Fig. 3) is inherently unstable. So, this amazing multistable behavior cannot be observed experimentally.

## IV. EXPERIMENTAL SETUP

Experimentally, the cw Ar laser beam ($\lambda=488$ nm) was focused to the crystal mounted on the cold finger of the He closed-cycle cryostat. The polarization of the light $E$ was parallel to the crystallographic axis $c$. The temperature in the cryostat was varied between 250 and 300 K using the temperature controller. The emitted light was focused onto the entrance slit of the monochromator and then detected with the visible-infrared photomultiplier tube (PMT). The chopper was placed before the monochromator to modulate the cw emission light. The detected modulated emission signal was amplified and averaged in the lock-in amplifier. The power of the Ar laser was slowly scanned from low to high and then back from high to low using the DIMENSION programmable controller. A typical scan took two to three hours. The diameter of the pumped spot, measured with the knife-edge technique, was equal to 0.65 mm. The emission intensity and Ar laser power were synchronously recorded by the computer. In the measurements of the transmitted power vs incident power, a power meter was placed behind the crystal. The power range in the scan depended on the sample and on the temperature of the cold finger, which was maintained with an accuracy $\pm1$ degree.

In the bistability experiment, we used two Cr:LiSGaF

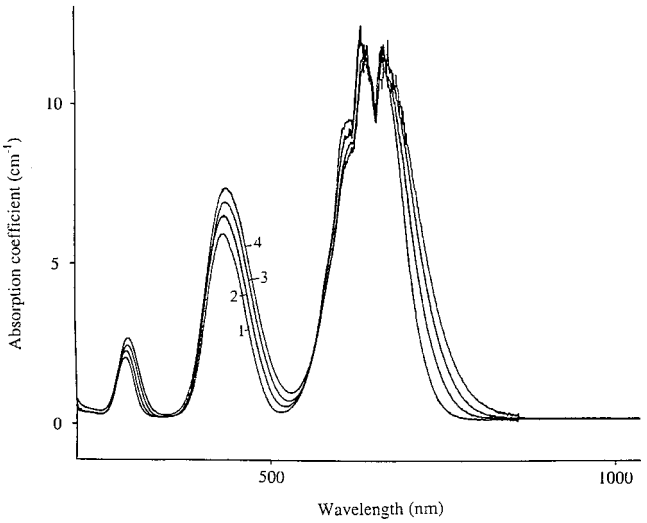


FIG. 8. Experimental absorption spectra of Cr(3%):LiSGaF at $E\parallel c$ at different temperatures: 1: room temperature, 2: 385 K, 3: 465 K, 4: 543 K.

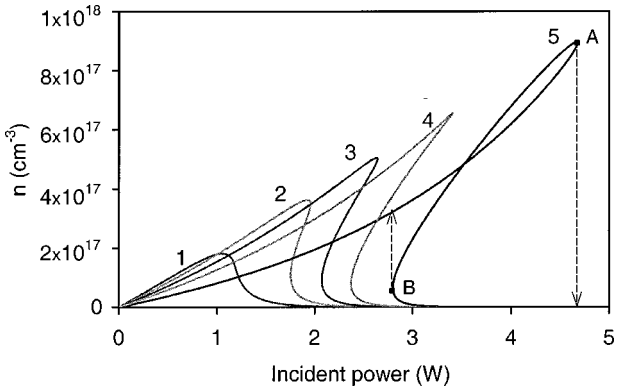


FIG. 10. Calculated excited state concentration vs incident pumping power at different temperatures $T_0$. 1: $T_0=300$ K, 2: $T_0=270$ K, 3: $T_0=250$ K, 4: $T_0=230$ K, 5: $T_0=200$ K; $\alpha=10^{-18}$ cm$^3$/s, $\lambda_p=488$ nm, $\chi=6\times10^{-3}$ W/deg, $l=0.1$ cm, $s=3.3\times10^{-3}$ cm$^2$, $n_{\mathrm{Cr}}=8.5\%$, $E\parallel c$.

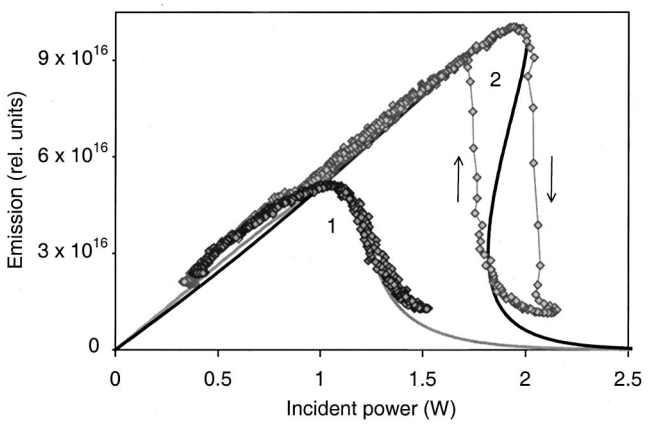


FIG. 11. Experimental emission intensity plotted vs pumping power in Cr(1.5%):LiSGaF (diamonds) and corresponding calculated curves (solid line) at $\chi=1.75\times10^{-3}$ W/deg, $\alpha=10^{-18}$ cm$^3$/s, $\lambda_p=488$ nm, $l=0.105$ cm, $s=3.3\times10^{-3}$ cm$^2$, $n_{\mathrm{Cr}}=2.1\%$, $E\|c$. 1: 300 K, 2: 270 K.

samples with Cr concentration equal to 1.5 and 20 %. The thickness of the samples was 1.05 and 0.75 mm, respectively.

### V. EXPERIMENTAL RESULTS AND DISCUSSION

In Fig. 11, the emission intensity in nominally 1.5%-Cr-doped LiSGaF is plotted versus the scanned incident pumping power. At room temperature, no hysteresis behavior has been found, while at $T=270$ K, the effect of intrinsic optical bistability has been observed. In the Cr(20%):LiSGaF crystal no hysteresis was observed at 300 and at 270 K, but it was present at 250 K. The fact that the bistability effect was observed at $T=270$ K in the Cr(1.5%):LiSGaF, but not in the Cr(20%):LiSGaF, is in line with our prediction that an efficient upconversion [(which is stronger in Cr(20%):LiSGaF than in Cr(1.5%):LiSGaF)] suppresses hysteretic behavior and bistability.

The hysteretic effect has been observed not only in the dependence $n(W_i)$, but also in the dependence of the transmitted power versus incident pumping power $W_t(W_i)$, Fig. 12. When we tried to fit the experiment scan curves with the calculated ones, a fairly good agreement was obtained at the

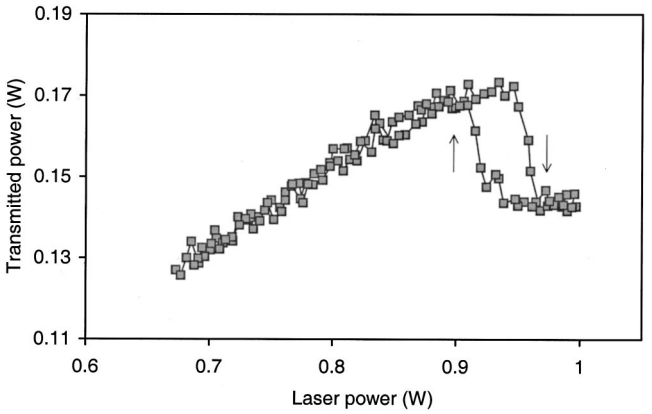


FIG. 12. Experimental transmitted power vs incident power in Cr(20%):LiSGaF.

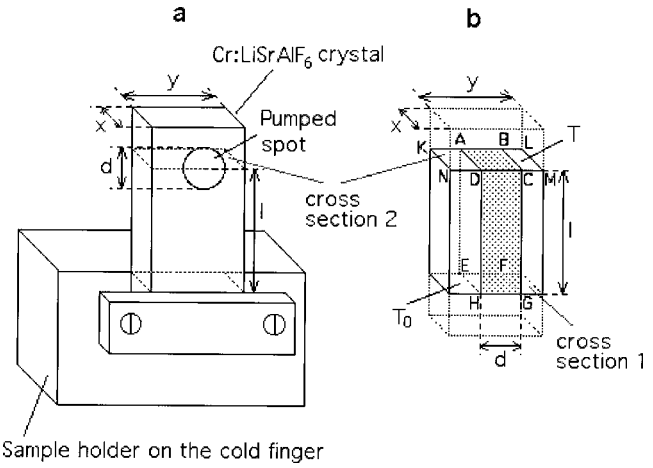


FIG. 13. (a) Schematic diagram of the sample holder with experimental sample. (b) Schematic diagram of the sample and several cross section planes and light propagation paths taken into account in the model.

value $\chi$ equal to $1.75\times10^{-3}$ W/deg ($\chi$ was the only fitting parameter in the system). All other parameters in the calculation were set to be equal to the experimental ones. (Absorption in nominally 1.5%-Cr-doped LiSGaF at $\lambda=488$ nm corresponded to $n_{\mathrm{Cr}}=2.1$ at.%.) The estimations showed that the value $\chi=1.75\times10^{-3}$ W/deg can be considered reasonable given the geometry of the experiment. The sample mounted in the sample holder on the cold finger of the cryostat is shown schematically in Fig. 13. We assumed that the thermal contact between the sample and the sample holder was perfect (a special silicon heat sink compound, No. 340 from Dow Corning, was used) and that the temperature in cross section 1 was equal to the temperature of the sample holder $T_0$ (Fig. 13). In the calculation of the factor $\chi$, we also assumed that heat was deposited inside the sample not along the actual trace of the laser beam, but in a very thin plain layer *ABCD* in the cross section 2, Fig. 13(b). The width of the layer was equal to the diameter of the pumped spot, $AB=d$. The position (height) of the cross section 2 corresponded to of the center of the pumped spot in Fig. 13(a). (Taking into account a large number of assumptions already taken in the model, the two new simplifying assumptions made seemed to be not inappropriate.) Under these assumptions, the minimum value of $\chi$,

$$\chi_{\min}=KS_{ABCD}/l=Kxd/l, \tag{5}$$

corresponds to the case when heat propagates only in the "column" *ABCDEFGH*. Here $K$ is the thermal conductivity coefficient, $S_{\mathrm{ABCD}}$ is the cross section area of the heat propagation path, and the dimensions $l$, $x$, and $d$ are shown in Fig. 13. Similarly, the maximum value of $\chi$ can be obtained under the assumption that heat propagates through the whole cross section of the sample *KLMN*,

$$\chi_{\max}=KS_{KLMN}/l=Kxy/l. \tag{6}$$

(The area $S_{KLMN}$ and the dimension $y$ are shown in Fig. 13.)

The values of the thermal conductivity coefficient in $Cr:LiSrGaF_6$ are equal to $3.6\times10^2$ W/(cm·deg) for propagation along the crystallographic axis **c** and $3.4\times10^2$ W/(cm·deg) for propagation perpendicular to the crystallographic axis **c** (the data are adopted from the catalog of VLOC, the company manufacturing $Cr:LiSrGaF_6$ crystals). In our calculations, we used the average value, $K=3.5\times10^2$ W/(cm·deg). Other experimental parameters were equal to $x=1.05$ mm, $y=2.55$ mm, $l=1.5$ mm, and $d=0.65$ mm. Substituting these numbers into Eqs. (5), (6), one gets $\chi_{max}=6.25\times10^{-3}$ W/deg and $\chi_{min}=1.6\times10^{-3}$ W/deg. Thus, the value $\chi=1.75\times10^{-3}$ W/deg, obtained from the best fit of calculation and experiment, agrees with the one obtained from the heat transfer considerations above. Taking into account a large number of simplifying assumptions taken in the calculations (in Sec. III), this is a fairly good quantitative agreement between the theory and the experiment, confirming the validity of our model.

Thus, we have demonstrated a good qualitative and quantitative agreement between the theory and the experiment. This validates our model and implies that the model can be used for accurate quantitative predictions of various other particularities of the bistability effects and hysteresis in Cr:LiSGaF and Cr:LiSAF laser-related crystals.

In principle, the same bistability effects can be expected in any luminescent material with strong dependence of the luminescence quantum yield on temperature. The question whether the temperature dependent nonlinearity in a given material is strong enough to produce bistability does not have an universal answer since the bistability also depends on many other experimental parameters, such as heat sink temperature, pumping wavelength, etc.

In the following analysis, for some given set of the system parameters, $T_0=250$ K, $\alpha=1\times10^{-18}$ cm$^3$/s, $\lambda_p=488$ nm, $\chi=6\times10^{-3}$ W/deg, $l=0.1$ cm, $s=3.3\times10^{-3}$ cm$^2$, we have calculated the series of traces $n(W_a)$ [Fig. 14(a)] corresponding to the family of curves $\tau(T)$ depicted in Fig. 14(b). Curve 3 in Fig. 14(b) is calculated according to Eq. (1) with the parameters $A$, $B$, and $\Delta E$ corresponding to those in Cr:LiSGaF. All other trial curves $\tau(T)$ in the same figure are calculated at the same value of $A$ but different values of $B$ and $\Delta E$. The five curves in Fig. 14(b) are characterized by the same value of $\tau$ at small temperatures, they bend approximately at the same temperature point ($\approx$50 °C) but have different temperature-dependent nonlinearities. As follows from Fig. 14(a), the bistability can be seen in traces 1–4 and (the hysteresis loop in trace 4 is marginally small) and not in trace 5. Thus, at the given set of experimental parameters, the bistability in the system can be observed at $\Delta E\geqslant4056$ cm$^{-1}$.

In Fig. 14(b), along with calculated trial traces, we plotted several experimental curves $\tau(T)$ corresponding to different representative laser materials (adopted from Ref. 18). As follows from this figure, Ti-sapphire and $Co^{2+}:MgF_2$ laser crystals have temperature dependent nonlinearities stronger than that in trace 4. Thus, an intrinsic optical bistability can be expected in these two materials. In ruby and Nd:ZBAN the temperature dependent nonlinearity is smaller than that in trace 4. Thus, at the given set of experimental parameters, the bistability in these two materials is unlikely. To conclude, the hysteretic and bistability phenomena similar to those found in Cr:LiSGaF crystals can be predicted in many solid-state laser materials although not in all of them.

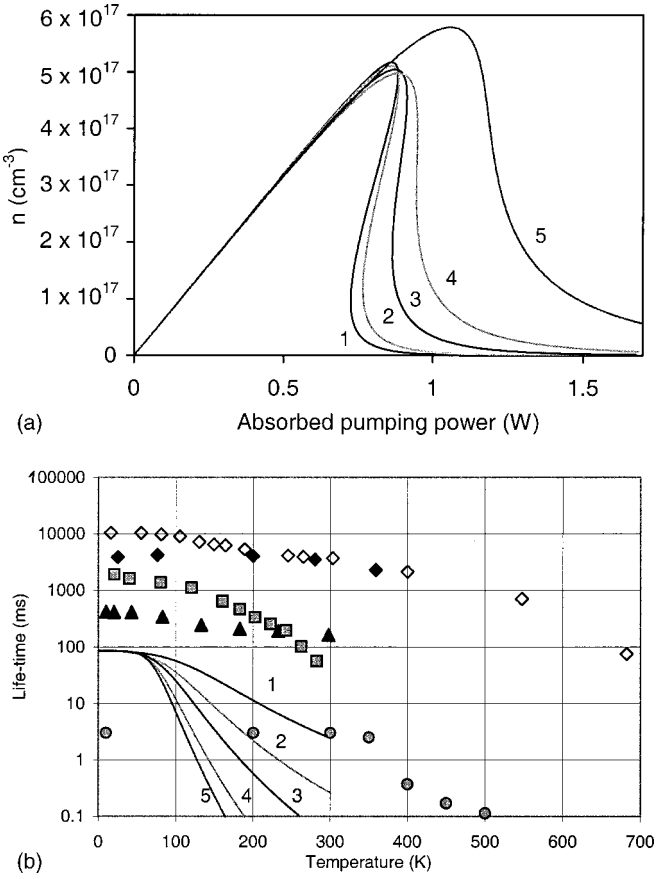


FIG. 14. (a) Excited state concentration $n$ calculated as a function of incident pumping power $W_a$ at different values of $B$ and $\Delta E$. 1: $B=1\times10^{18}$, $\Delta E=7696$ cm$^{-1}$, 2: $B=1\times10^{16}$, $\Delta E=6656$ cm$^{-1}$, 3: $B=8\times10^{12}$, $\Delta E=5054$ cm$^{-1}$ (LiSGaF), 4: $B=1\times10^{11}$, $\Delta E=4056$ cm$^{-1}$, 5: $B=1\times10^{9}$, $\Delta E=3120$ cm$^{-1}$. (b) Luminescence lifetimes plotted versus temperature. Solid lines: theoretical curves calculated using Eq. (1) with different values of $B$ and $\Delta E$. [The values of $B$ and $\Delta E$ used to calculate curves 1–5 in (b) correspond to the values used to calculate the curves 1–5 in (a).] 1: $B=1\times10^{18}$, $\Delta E=7696$ cm$^{-1}$, 2: $B=1\times10^{16}$, $\Delta E=6656$ cm$^{-1}$, 3: $B=8\times10^{12}$, $\Delta E=5054$ cm$^{-1}$, (LiSGaF), 4: $B=1\times10^{11}$, $\Delta E=4056$ cm$^{-1}$, 5: $B=1\times10^{9}$, $\Delta E=3120$ cm$^{-1}$. Open diamonds: optically thick ruby sample, filled diamonds: optically thin ruby sample, squares: $Co^{2+}:MgF_2$, triangles: Nd:ZBAN, circles: $Al_2O_3:Ti^{3+}$ (Ref. 18).

## VI. SUMMARY AND CONCLUSIONS

An intrinsic optical bistability based on a thermal nonlinearity has been theoretically predicted in $Cr^{3+}:LiSrGaF_6$ and $Cr^{3+}:LiSrAlF_6$ laser-related crystals. A model demonstrating a hysteresis in the dependence of steady state luminescence intensity and transmission versus pumping intensity has been developed.

It has been found that the size of the hysteresis loop increases with the decrease of the heat sink temperature (thermal bath) $T_0$, that the energy transfer upconversion suppresses the hysteresis, and that the hysteretic loop becomes larger when the pumping frequency $\nu_p$ is getting closer to the emission frequency $\nu_e$. The heat sink rate $\chi$ influences the size of the emission vs. pumping curve, but not its characteristic shape.

The temperature dependence of the $Cr^{3+}$ luminescence lifetime in Cr:LiSGaF and Cr:LiSAF laser-related crystals has been experimentally studied. The expression describing the luminescence relaxation rate at different temperatures has been found.

An intrinsic optical bistability in the luminescence and the transmitted power has been experimentally observed in Cr:LiSGaF.

A good qualitative and quantitative agreement between the theory and the experiment has been demonstrated.

---

*Email address: mnoginov@nsu.edu, FAX: (757) 823-9054.

[1] H. M. Gibbs, S. L. McCall, and T. N. C. Venkatesan, Phys. Rev. Lett. **36**, 1135 (1976).

[2] C. M. Bowden and C. C. Sung, Phys. Rev. A **19**, 2392 (1979).

[3] C. M. Bowden and J. P. Dowling, Phys. Rev. A **47**, 1247 (1993).

[4] M. E. Crenshaw and C. M. Bowden, Phys. Rev. A **53**, 1139 (1994).

[5] M. P. Hehlen, H. U. Güdel, Q. Shu, J. Rai, S. Rai, and S. C. Rand, Phys. Rev. Lett. **73**, 1103 (1994).

[6] M. P. Hehlen, H. U. Güdel, Q. Shu, and S. C. Rand, J. Chem. Phys. **104**, 1232 (1996).

[7] M. P. Hehlen, A. Kuditcher, S. C. Rand, and S. R. Lüthi, Phys. Rev. Lett. **82**, 3050 (1999).

[8] S. R. Lüthi, M. P. Hehlen, T. Riedener, and H. U. Güdel, J. Lumin. **76&77**, 447 (1998).

[9] M. A. Noginov, G. B. Louts, C. Steward, B. Lucas, D. Fider, V. Peters, G. Huber, and C. M. Bowden, in *Nonlinear Optics: Materials, Fundamentals and Applications*, OSA Technical Digest (Optical Society of America, Washington, D.C., 2000), pp. 405–407.

[10] L. K. Smith *et al.*, IEEE J. Quantum Electron. **28**, 2612 (1992).

[11] S. A. Payne *et al.*, Appl. Opt. **33**, 5526 (1994).

[12] D. Kopf *et al.*, Appl. Phys. B: Lasers Opt. **65**, 235 (1997).

[13] I. T. Sorokina *et al.*, Appl. Phys. B: Lasers Opt. **65**, 245–254 (1997).

[14] M. Stadler *et al.*, in *OSA Proceedings on Advanced Solid-State Lasers*, edited by George Dubé and Lloyd Chase, Vol. 10 of OSA Proceedings Series (Optical Society of America, Washington, D.C., 1991), pp. 18–20.

[15] M. A. Noginov, *et al.*, in *OSA Proceedings on Advanced Solid-State Lasers* (Ref. 14), pp. 21–24.

[16] J. M. Eichenholz and M. Richardson, IEEE J. Quantum Electron. **34**, 910–919 (1998).

[17] M. A. Noginov *et al.*, in *OSA Proceedings on Advanced Solid-State Lasers*, edited by Albert A. Pinto and Tso Yee Fan, Vol. 15 of OSA Proceedings Series (Optical Society of America, Washington D.C., 1993), pp. 376–380.

[18] R. C. Powel, *Physics of Solid-State Laser Materials* (Springer-Verlag, New York, 1998), p. 423.